Prediction of Internal Defect Area in Wooden Components by Stress Wave Velocity Analysis

Xin Li,[a,c] Jian Dai,[b,c,*] Wei Qian,[b,c] and Li-Hong Chang [a]

In this study, wooden components torn down from ancient buildings were used as the experimental materials. With methodology based on reverse simulation testing, some artificial holes making up different proportional areas of their cross-section were chiseled and tested with a six-sensor-point stress wave testing device. The results indicated that two-dimensional analog images could be used to judge the internal defects of wooden components qualitatively but did not provide quantitative, accurate determination. By comparing and contrasting the attenuation tendency of stress wave velocities among adjacent sensor points, separated sensor points, and diagonal sensor points, the defect grade of wooden components can be classified. Six variations were chosen as discriminant factors. These were the attenuation coefficients of the stress wave velocities *via* three propagation paths and the relative proportions of their absolute values. The Mahalanobis distance discrimination model was adopted for the in-grade estimation of the internal defects present in the component's cross-section. This method had high operability and no misjudgment ratio.

Keywords: Ancient buildings; Wooden components; Stress wave; Internal defects; Distance discrimination

*Contact information: a: College of Architecture and Civil Engineering, Beijing University of Technology, Beijing, 100124, China; b: College of Architecture and Urban Planning, Beijing University of Technology, Beijing, 100124, China; c: Beijing Research Center of Historic Building Protection Engineering, Beijing, 100124, China; *Corresponding author: 67393299@sina.com*

INTRODUCTION

Ancient Chinese buildings were mostly built with wood (Ma 2003). The relevant literature shows that China has 1,080 historic building complexes that are listed as protected sites, more than half of which are timber frame buildings (Yin and Yamamoto 2013). The preferred species of timber for buildings during the Ming and Qing Dynasties (1368AD-1911AD) in the Beijing district included Chinese pine (*Pinus tabulaeformis* Carr.), fir (*Abies fabri* (Mast.) Craib), spruce (*Picea asperata* Mast.), larch (*Larix gmelinii* Kuzen.), and others (Liu 2006).

The timber frame has many outstanding merits, such as light weight, large span, replaceable components, and good earthquake resistance, *etc.* (Fig.1). But as an anisotropic biological material, wood has a very complex internal structure and suffers internal defects easily under natural conditions, such as holes, rot, and decay (Zhang *et al*. 2011). Outdoor environmental effect (exposure to radiation, moisture, and temperature changes, the worms and termites infestation, *etc.*), artificial damage (damage caused by wars, impertinent repairing work, *etc.*), and biodegradation resulting from its material characteristics are considered to be the most important causes of these defects, and these defects can give rise to the cross-section weakening of the wooden components (Yang *et al*. 2012). Like many other building structural styles, the effective cross-section weakening of wooden

components can make them lose the bearing capacity and even reduce the reliability of the whole building (Li *et al*. 2005). Thus, during the structural health monitoring and assessment of the ancient timber buildings, it is important to determine the internal conditions of the wooden components without damaging them (Duan *et al*. 2007), and some fundamental data could make it possible to quickly and precisely estimate the state of internal defect of wooden components for the renovation of a historic building (Wang 2006; Xu and Qiu 2011).

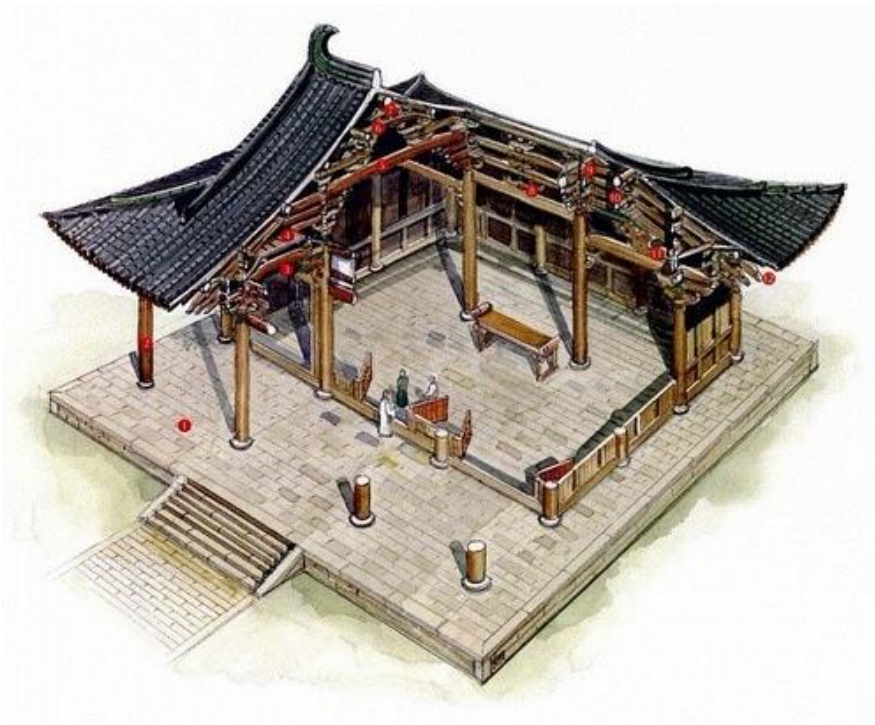

Fig. 1. Example of an ancient Chinese timber frame building

The non-destructive testing (NDT) techniques are effective ways to provide valuable information on the state of the material, and to improve the quality of the diagnosis of many structures, *e.g.* steelwork, concrete, and timber (Balayssac *et al.* 2011). Among these techniques, stress wave tomography is one of the mature NDT methods widely used in timber structure testing (Huang *et al*. 2007). It provides a planar image of a timber cross-section through matrix transformation with image reconstruction. If any cross-sectional weakening exists in the measured object, it can be obviously mapped on the PC screen. The principle of stress wave testing is based on differences in the velocity of stress waves propagating in different materials, since the velocity of sound in healthy wood is much higher than in voids or in decaying wood (Halabe *et al.* 1997; Wang *et al.* 2004; Feng and Li 2008). Several studies of this technology have been performed, both experimentally and with simulations (Kiernan 2009). These studies have indicated that stress wave testing can effectively diagnose the defects in the wood (Liang 2008). The defect situation of wooden components can be deciphered by comparing the propagation velocities of stress waves through the components *via* different paths.

The objective of this study is to predict the internal defect of wooden components more accurately by using the statistical approaches of the stress wave propagation. Several statistical approaches have been based on the measured data of NDT and used in structural

health monitoring and assessment, *e.g.* neural networks (Sohn *et al*. 2002), fuzzy pattern recognition (Taha and Lucero 2005), an autoregressive model (Figueiredo *et al.* 2011), and Malanalobis distance discrimination (Atsushi and Akira 2004). This study used wooden components acquired while repairing ancient buildings as the experimental material, and the artificial holes were chiseled to simulate the cross-sectional weakening. The attenuation law of stress wave velocity through different propagation paths and different proportions of holes were analysed, and the discriminative and ratio relationships using the Mahalanobis distance discriminant model were established.

Distance discrimination is a frequently used statistical analysis method that determines the internal conditions of a sample based on analysis of its property parameters (Luo *et al.* 2013). The basic principle is to determine and classify a sample according to its regularity and data distribution of the sample as well as statistical information of other known samples. The purpose of this methodology is to classify a sample into an ensemble (Gong *et al.* 2007).

The work will serve some parameter for future stress wave inspection and help to determine the presence of internal defects in wooden components more quickly and precisely during on-site ancient building repair.

EXPERIMENTAL

Basic Information on Materials Used for Testing

The experimental material used in this study was a column disassembled from an ancient building repair project with homogeneous internal material and no obvious decay or defect (some tiny nonpenetrating drying cracks existed in the surface, their effect was neglected in this study), as judged by preliminary testing (knocking on the surface and examining the appearance of the sawed section) (Fig. 2). Before cutting into the specimens, some basic data were measured: the cross-section was approximately a circle with a diameter of 280 mm; an average surface moisture content of 16.7% was measured by the KT-50 Wood Moisture Meter (KLORTNER Technology Co., Ltd, Italy); the testing material did not have an intonaco layer (a surface coating of the wooden components made from plaster and hemp fiber to protect it), and its species was determined to be Chinese pine.

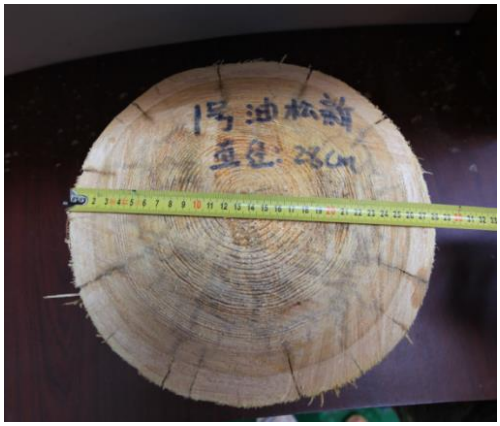

Fig. 2. The experimental material disassembled from an ancient building

Experimental Procedures and Methods

Six cylinders were cut from the experimental material with heights of 100 mm, numbered 1 to 6. Specimens 1 to 5 were for data collection, and specimen 6 was for verification of the results.

The testing device used for data collection was an FAKOPP 3D Acoustic Tomograph (FAKOPP Enterprise, Hungary). The Fakopp 3D device used several sensors and measured the travel times between each sensor pair by tapping them. The travel times measured by the Fakopp 3D were transmitted to the software on the PC. This software calculated the resulting two-dimensional velocity map of the internal state of the measured object. In this experiment, six sensors were uniformly located in the direction of the cylinder's perimeter and nailed into the wood 10 to 15 mm deep.

The average moisture content of the specimens was adjusted to roughly 12% in an RGQ Artificial Climate Box (SENXIN Experimental Instrument Co., Ltd., China), similar to that of the wooden components of buildings under natural conditions. First, cross-section analog images were collected by the tomograph, and the stress wave velocities were classified into three types according to their different propagation paths, including the velocity between adjacent sensor points, V_{a12}, V_{a23}, V_{a34}, V_{a45}, and V_{a56}, their mean value recorded as V_{a0}; the velocity between separate sensor points, V_{b13}, V_{b24}, V_{b35}, V_{b46}, V_{b51}, and V_{b62}, their mean value recorded as V_{b0}; and the velocity between diagonal sensor points V_{c14}, V_{c25}, and V_{c36}, the mean value of which was recorded as V_{c0}, as shown in Fig. 3. V_{a0}, V_{b0}, and V_{c0} were the baseline values of the stress wave velocity along the three propagation paths.

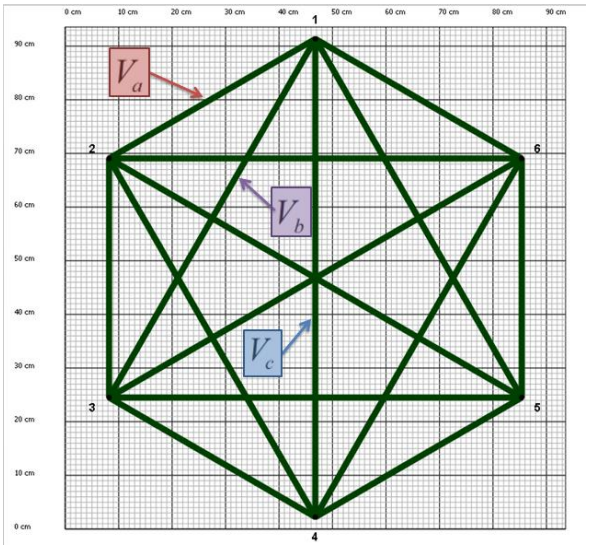

Fig. 3. Three propagation paths of stress wave velocities among the timber cross-section

Next, penetrating holes were artificially chiseled from the geometric centre of the specimen's cross-section, and the stress wave velocities V_a, V_b, and V_c were collected by tapping the sensors. The areas of the holes were enlarged in a stepwise manner. The hole proportions were in multiple relationship, for which the areas were 1/32*S*, 1/16*S*, 1/8*S*, 1/4*S*, and 1/2*S*, respectively, where *S* represents the cross sectional area of the specimen (*S ca.* 616 cm^2), and the corresponding diameters of the holes were 50 mm, 70 mm, 100 mm, 140 mm, and 200 mm, respectively (in consideration of the manual error, the sizes were measured within a centimeter).

A comparison between the actual area of the chiseled holes (*R*) and the analog imaging area as determined by the tomograph (*T*) is shown in Fig. 4.

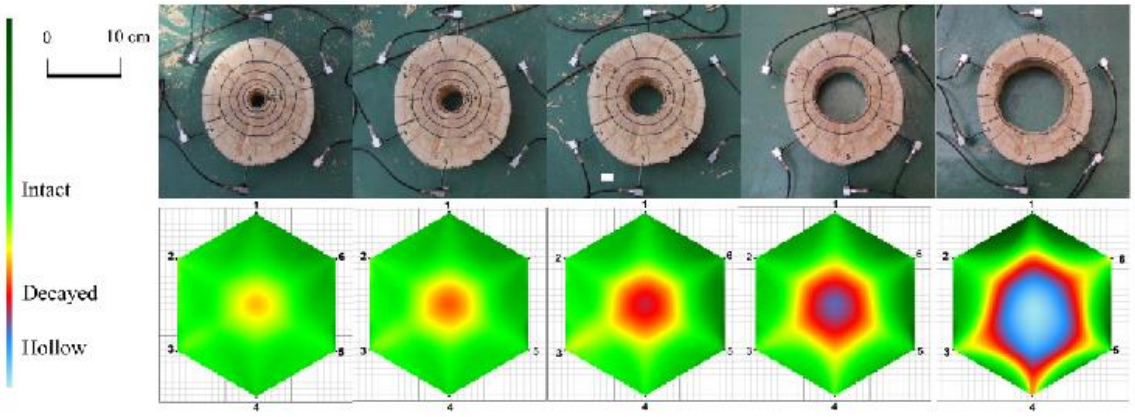

Fig. 4. Comparison of actual hole area and imaged area by stress waves

RESULTS AND DISCUSSION

Analysis of Testing Hole Area

The working principle of FAKOPP 3D is to establish a fitting relationship for velocity and color, in which different velocities correspond to different colors. High velocity corresponds to healthy wood, and low velocity corresponds to hollow wood. After the calculation by FAKOPP 3D software, an analog image of the wooden cross-section is prepared to show the results with gradual changes in color. The color progression of "Green-Red-Blue" corresponds to the internal state in form of "Intact-Decayed-Hollow," respectively, as shown by the legend in Fig. 4. In FAKOPP 3D software, the default critical values of velocities corresponding to different internal state come from the reference database with different tree species. (In the present study, the reference data of "Chinese (red) pine" was chosen).

Based on the default critical values of the corresponding tree species, the analog images distinctly revealed the proportion of the holes, but with large error. The smaller the proportion of the hole was, the larger the margin of error was; the highest average margin of error was 69%.The average testing data of specimens 1 through 5 are indicated by Table 1. With the default parameters of the stress wave testing software, the analog images lacked the ability to provide quick, accurate, quantitative judgment.

Table 1. Comparison of Testing Area (*T*) and Actual Hole Area (*R*)

Hole Proportion	Testing Area (*T*) (cm^2)	Actual Hole Area (*R*) (cm^2)	Margin of Error
1/32*S*	61.50	19.22	69%
1/16*S*	98.40	38.44	60%
1/8*S*	141.45	76.88	46%
1/4*S*	202.95	153.75	24%
1/2*S*	246.00	307.50	11%

Analysis of the Law of Stress Wave Velocity Attenuation

To determine the degree of internal defects in wooden cross-sections, the key element in the tomograph's ability is to explore and analyze the propagation velocities of stress waves inside wooden cross-sections. The data analysis is shown in Table 2. It shows that there were no noticeable differences of ranges among the velocities along the three propagation paths (V_a, V_b, V_c) under the initial state, with no defects (An 2013). The maximum was 1321 m/s, the minimum was 1146 m/s, the standard deviation was 43.31, and the coefficient of variation (CV) was 3.48%. The mean velocities of the three propagation paths were calculated as V_{a0} = 1255 m/s, V_{b0} = 1239 m/s, and V_{c0} = 1243 m/s, the baseline velocities. On this basis, the attenuation values and ratios of velocity compared with the baseline can be obtained.

Table 2. Data Analysis of Stress Wave Velocity Propagation

Test Condition	Velocity	Maximum (m/s)	Minimum (m/s)	Standard Deviation	CV (%)	Attenuation (m/s)	Attenuation Coefficient δ (%)
No Defect	V_a	1301	1193	43.31	3.48	0	0
	V_b	1268	1173			0	0
	V_c	1321	1146			0	0
1/32S Defect	V_a	1262	1177	66.60	5.63	32	2.55
	V_b	1249	1148			21	1.70
	V_c	1140	1022			137	11.02
1/16S Defect	V_a	1272	1169	92.08	7.95	28	2.23
	V_b	1234	1110			39	3.15
	V_c	1092	954			197	15.85
1/8S Defect	V_a	1260	1159	127.45	11.42	33	2.63
	V_b	1206	1089			67	5.41
	V_c	1011	861			289	23.25
1/4S Defect	V_a	1256	1171	182.16	17.65	40	3.19
	V_b	1130	997			165	13.32
	V_c	892	708			436	35.08
1/2S Defect	V_a	1099	1018	215.43	26.28	197	15.70
	V_b	911	806			389	31.40
	V_c	590	515			691	55.59

Along with the expansion of the cross sectional holes area, the average velocities along the three propagation paths all had an attenuation tendency, but in different rates. V_c had the fastest attenuation rate and V_a had the slowest. The reason is that the propagation path V_c is through the geometric center of the wooden cross-sections; if a hole is present, then the sound has to travel a longer distance. This means a higher travel time; hence the velocities between the diagonal sensors are slow down obviously. Both the standard deviation and variable coefficient tended to increase, where the maximum values were 215.43 and 26.28%, respectively. It could hence be estimated that the absolute differences of the velocities along the three propagation paths increased when the cross sectional hole area was increased. The attenuation coefficient δ_m were calculated as follows,

$$\delta_m = \frac{v_{m0} - v_{mk}}{v_{m0}} \times 100\% \quad (1)$$

where v_{m0} (m =a, b, c) are the mean velocities of the three propagation paths under the initial state with no defects, and v_{mk} (m=a, b, c ; k=1, 2, 3, 4, 5) are the mean velocities of the three propagation paths under the state with 1/32S, 1/16S, 1/8S, 1/4S, 1/2S (S is the cross sectional area of the specimens) hole proportions, respectively.

Relations of Wave Velocity Classification

From the analysis above, different attenuation trends were observed in each of the three propagation paths. When the attenuation coefficient of the stress wave velocity (ACV) (δ_m) exceeds 10%, the given proportions of holes are considered to have a noticeable impact on the propagation path. The relevant study shows that the stress wave velocities in three propagation paths are evidently correlated with the area proportion of the holes in the cross-section (An 2013). From this correlation, a relationship between them was established to promptly determine the defect area in a wooden component's cross-section (Table 3).

Table 3. Judgment of Defect Area by ARV of Different Propagation Paths

Test Condition	δ_a	δ_b	δ_c
No Defect	-	-	-
Defect Area ≤ 1/32S	-	-	+
Defect Area ≤ 1/16S	-	-	+
Defect Area ≤ 1/8S	-	-	++
Defect Area ≤ 1/4S	-	+	++
Defect Area ≤ 1/2S	+	++	+++
"-" represents ACV ≤ 10%; "+" represents 10% < ACV ≤ 20%; "++" represents 20% < ACV ≤ 50%; and "+++" represents ACV > 50 %.			

Prediction of Defect Area by Distance Discrimination Model

To determine the defect area more precisely in this study, Mahalanobis distance discrimination was adopted to analyze and predict the internal condition of wooden sections. The Mahalanobis distance discriminant model, using a deductive process, is described below.

Let the totality $G = [X_1, X_2, \ldots X_k]^T$ be a k-dimensional totality (inspect k items of discriminant factors) and sample $X = [x_1, x_2, \ldots x_k]^T$. Let $\mu_i = E(X_i)$ (i = 1, 2, … k). Then, the average vector quantity of the totality $\mu = (\mu_1, \mu_2, \ldots \mu_k)^T$. The covariance matrix of totality G is

$$\Sigma = \mathrm{Cov}(G) = E[(G - \mu)(G - \mu)^T] \quad (2)$$

Assuming $\Sigma > 0$ (Σ is a positive definite matrix), the Mahalanobis distance between two samples X_i, X_j (i = 1, 2, … k; j = 1, 2, … k) is defined as

$$d^2(X_i, X_j) = (X_i - X_j)^T \Sigma^{-1} (X_i - X_j) \quad (3)$$

and the Mahalanobis distance from sample X to totality G is defined as

$$d^2(X, G) = (X - \mu)^T \Sigma^{-1} (X - \mu) \quad (4)$$

Assume there is a pth k-dimensional totality G_1, G_2, … G_p whose average vector quantities are $\mu_1, \mu_2, \ldots \mu_p$ and covariance matrices are $\Sigma_1, \Sigma_2, \ldots \Sigma_p$. Choosing any given k-dimensional sample $X = [x_1, x_2, \ldots x_k]^T$ and comparing the Mahalanobis distance from the

sample to each totality by calculating, the sample can be classified to one totality that has the least Mahalanobis distance. The basis for this classification is if

$$d^2(X, G_i) = \min[d^2(X, G_i)] \ (i=1, 2, \ldots k) \quad (5)$$

then,

$$X \in G_i. \quad (6)$$

Based on Mahalanobis distance discrimination, G is the grade of internal defects in a specimen's cross-section. G is divided into six classes, as shown in Table 4.

Table 4. Discrimination Grades and Standard

Grade of Internal Defect (G)	Discrimination Standard
G_0	No Defect
G_1	Defect area less than or equal 1/32S
G_2	Defect area less than or equal 1/16S
G_3	Defect area less than or equal 1/8S
G_4	Defect area less than or equal 1/4S
G_5	Defect area less than or equal 1/2S

Next, using MATLAB, six discriminant factors were chosen as follows: $\delta_a(X_1)$, $\delta_b(X_2)$, $\delta_c(X_3)$, $V_a/V_b(X_4)$, $V_b/V_c(X_5)$, and $V_a/V_c(X_6)$. Taking specimens 1 to 5 as the studied samples, some predictions were made to classify the internal defect holes of the specimens based on different proportional areas. Specimen 6 was used as the testing sample, and the accuracy of this discrimination method was verified. The results of the discrimination are shown in Table 5. By comparing the result of discriminant with the grand of actual internal defect, the results corresponded with the real situation perfectly, and that the misjudgment rate was 0, fully illustrating the rationality and effectiveness of predicting the internal defect area of wooden components with the distance discriminant model on the basis of the law of attenuation of stress wave velocities. This model is simple and effective in that it has a strong discriminant capability for estimating the internal defect area of wooden component sections and eliminates the influence of human factors (Shi *et al.* 2013).

CONCLUSIONS

1. Two-dimensional software-derived analog images of the stress wave detector distinctly showed the conditions of the internal section of the wooden components and allowed qualitative conclusions regarding defect positions and sizes. Large error existed in the quantitative predictions of the specific areas of the defects. The smaller the area of the defects was, the larger the margin of error was. The largest error was as high as 69%.
2. The law of attenuation of stress wave velocities via three propagation paths had clear relationships with the defect area in the wooden component sections. Along with the expansion of the cross sectional holes area, all the velocities had an attenuation tendency, for which V_c had the fastest attenuation rate and V_a had the slowest. The maximum values of standard deviation and variable coefficient were 215.43 and

26.28%, respectively. When velocity propagates in a certain path, compared to the velocity through defect-free wood, there is over 10% attenuation, and the defect area can be considered to influence the propagation velocity in that path. A quick determination of the internal defect area of the section can be achieved by making a comprehensive comparison of the attenuation relations in three propagation paths.

3. Using six discriminant factors, including the attenuation coefficient of stress wave velocity in three propagation paths and their ratios, the Mahalanobis distance discriminant model had fundamentally no misjudgment rate. The reverse simulation testing with artificial damage can give some effective statistical approach and fundamental data for the future stress wave inspection during the on-site work.

Table 5. Result of Discrimination by Mahalanobis Distance Discriminant Model

Specimen Number	Discriminant Factor						Grade of Internal Defect	Result of Discriminant
	$\delta_a(X_1)$ (%)	δ_b (X_2) (%)	δ_c (X_3)(%)	$V_a/V_b(X_4)$	V_b/V_c (X_5)	V_a/V_c (X_6)		
No. 1	0	0	0	1.0171	1.0236	1.0410	No Defect	G_0
No. 2	0	0	0	1.0232	0.9837	1.0065		G_0
No. 3	0	0	0	1.0008	0.9945	0.9953		G_0
No. 4	0	0	0	0.9984	1.0201	1.0185		G_0
No. 5	0	0	0	1.0079	1.0072	1.0151		G_0
No. 6	0	0	0	1.0309	0.9553	0.9849		G_0
No. 1	1.34	2.13	10.82	1.0253	1.1233	1.1517	Defect area less than or equal 1/32S	G_1
No. 2	2.19	1.49	9.62	1.0160	1.0721	1.0893		G_1
No. 3	3.33	2.07	10.27	0.9878	1.0854	1.0722		G_1
No. 4	3.79	1.97	10.86	0.9799	1.1218	1.0993		G_1
No. 5	0.94	1.42	10.76	1.0128	1.1125	1.1268		G_1
No. 6	3.46	1.03	13.70	1.0056	1.0956	1.1018		G_1
No. 1	2.01	5.37	16.75	1.0532	1.1635	1.2254	Defect area less than or equal 1/16S	G_2
No. 2	2.27	1.49	13.94	1.0151	1.1259	1.1430		G_2
No. 3	3.17	3.73	17.93	1.0066	1.1665	1.1742		G_2
No. 4	1.97	3.31	12.15	1.0122	1.1227	1.1364		G_2
No. 5	1.73	2.61	14.58	1.0171	1.1483	1.1679		G_2
No. 6	2.23	2.22	19.61	1.0308	1.1620	1.1977		G_2
No. 1	2.85	7.16	24.87	1.0643	1.2648	1.3461	Defect area less than or equal 1/8S	G_3
No. 2	3.24	4.39	22.25	1.0355	1.2096	1.2526		G_3
No. 3	1.67	5.48	25.51	1.0412	1.2619	1.3139		G_3
No. 4	2.84	4.57	20.19	1.0165	1.2198	1.2399		G_3
No. 5	1.81	4.59	19.44	1.0373	1.1929	1.2374		G_3
No. 6	3.15	6.10	27.25	1.0633	1.2331	1.3111		G_3
No. 1	1.88	15.00	38.22	1.1745	1.4082	1.6540	Defect area less than or equal 1/4S	G_4
No. 2	2.83	10.27	30.73	1.1090	1.2741	1.4129		G_4
No. 3	3.79	14.69	42.97	1.1304	1.4875	1.6814		G_4
No. 4	5.32	12.38	28.24	1.0819	1.2455	1.3475		G_4
No. 5	2.41	10.60	29.32	1.1009	1.2740	1.4025		G_4
No. 6	3.58	16.88	40.80	1.1973	1.3414	1.6061		G_4
No. 1	13.41	31.29	53.49	1.2816	1.5122	1.9381	Defect area less than or equal 1/2S	G_5
No. 2	17.57	32.64	55.09	1.2522	1.4755	1.8475		G_5
No. 3	14.84	32.96	55.53	1.2713	1.4991	1.9059		G_5
No. 4	16.11	31.70	58.57	1.2263	1.6816	2.0621		G_5
No. 5	13.74	32.12	52.99	1.2809	1.4542	1.8627		G_5
No. 6	18.45	27.81	57.46	1.1647	1.6210	1.8879		G_5

ACKNOWLEDGMENTS

The authors are grateful for the support of the National Key Technology Support Program of China (2013BAK01B03) and the National Natural Science Foundation of China (51278003).

REFERENCES CITED

An, Y. (2013). *Two-Dimensional Imaging Technique of Wood Defects Based on Stress Wave*, Ph.D. dissertation, Chinese Academy of Forestry, Beijing, China.

Atsushi, I., and Akira, T. (2004). "Delamination identification of CFRP structure by discriminant analysis using Mahalanobis distance," *Key Engineering Materials* 270-273, 1859-1865. DOI: 10.4028/www.scientific.net/KEM.270-273.1859

Balayssac, J. P., Laurens, S., Breysse, D., and Garnier, V. (2011). "Evaluation of concrete properties by combining NDT methods," *Nondestructive Testing of Materials and Structures* 6,187-192.DOI: 10.1007/978-94-007-0723-8_27

Duan, X. F., Wang, P., Zhou, G. W., and Gao, C. Y. (2007). "Nondestructive evaluation of dynamic MOE of ancient wooden structure members by stress wave method," *Journal of Northwest Forestry University* 22(1), 112-114. DOI: 10.3969/j.issn.1001-7461.2007.01.031

Feng, H. L., and Li, G. H. (2008). "Stress wave propagation modeling in wood non-destructive testing," *2008 Asia Simulation Conference - 7th International Conference on System Simulation and Scientific Computing*, 10-12 October, Beijing, pp. 1441-1445. DOI: 10.1109/ASC-ICSC.2008.4675601

Figueiredo, E., Figueiras, J., Park, G., Farrar, C. R., and Worden, K. (2011). "Influence of the autoregressive model order on damage detection," *Computer-Aided Civil and Infrastructure Engineering* 26(3), 225-238. DOI: 10.1111/j.1467-8667.2010.00685.x

Gong, F. Q., and Li, X. B. (2007). "A distance discriminant analysis method of forecast for shaft-lining non-mining fracture of mine," *Journal of China Coal Society* 32(7), 700-704. DOI: 10.3321/j.issn:0253-9993.2007.07.006

Halabe, U. B., Bidigalu, G. M., Ganga Rao, H. V. S., and Ross, R. J. (1997). "Nondestructive evaluation of green wood using stress wave and transverse vibration techniques," *Materials Evaluation* 55(9), 1013-1018.

Huang, R. F., Wang, X. H., Li, H., and Liu, X. Y. (2007). "Quantitative analysis on the detected results by resistograph on inside wood defect of ancient architecture," *Journal of Beijing Forestry University* 29(6), 167-171. DOI: 10.3321/j.issn:1000-1522.2007.06.028

Kiernan, S., Cui, L., and Gilchrist, M. D. (2009). "Propagation of a stress wave through a virtual functionally graded foam," *International Journal of Non-Linear Mechanics* 44(5), 456-468. DOI: 10.1016/j.ijnonlinmec.2009.02.006

Li, T. Y., Wei, J. W., Zhang, S. Y., and Li, S. W. (2005). "Appraisal on the structure of the Yingxian wooden tower," *China Civil Engineering Journal* 38(02), 51-58. DOI: 10.3321/j.issn:1000-131X.2005.02.009

Liang, S. Q. (2008). *Study on Diagnosis and Assessment Technology of Stress Wave Tomography in Old and Famous Trees*, Ph. D. dissertation, Chinese Academy of Forestry, Beijing, China.

Liu, W. B. (2006). *Study on Relationship of Molder Condition between Variations of Chemic Ingredients and Bending Strength of Ancient Wood Structure in the Imperial Palace*, M.S. thesis, Beijing Forestry University, Beijing, China.

Luo, Z. G., Li, X. D., Zhao, J. L., and Zhang, J. J. (2013). "Crack accurate identification by using Mahalanobis distance discrimination method," *Journal of Vibration and Shock* 32(21), 186-188. DOI: 10.3969/j.issn.1000-3835.2013.21.032

Ma, B. J. (2003). *Wood Construction Techniques of Ancient Chinese Architecture*, Science Press, Beijing, China.

Shi, H. T., Liu, J. C., Xue, P., Zhang, K., Wu, Y. H., Zhang, L. X., and Tan, S. (2013). "Improved relative-transformation principal component analysis based on Mahalanobis distance and its application for fault detection," *Acta Automatica Sinica* 39(9), 1533-1542. DOI: 10.3724/SP.J.1004.2013.01533

Sohn, H. Worden, K. and Farrar, C. R. (2002). "Statistical damage classification under changing environmental and operational conditions," *Journal of Intelligent Material Systems and Structures* 13(9), 561-574. DOI: 10.1106/104538902030904

Taha, M. R., and Lucero, J. (2005). "Damage identification for structural health monitoring using fuzzy pattern recognition," *Engineering Structures* 27(12), 1774-1783. DOI: 10.1016/j.engstruct.2005.04.018

Wang, X. P., Ross, R. J., Green, D. W., Brashaw, B., Englund, K., and Wolcott, M. (2004). "Stress wave sorting of red maple logs for structural quality," *Wood Science and Technology* 37(6), 531-537. DOI: 10.1007/s00226-003-0202-8

Xu, M. G., and Qiu, H. X. (2011). "Experimental study on properties of aged wood of ancient architecture," *Earthquake Resistant Engineering and Retrofitting* 33(4), 53-55. DOI: 10.3969/j.issn.1002-8412.2011.04.009

Yang, N., Li, P., Law, S. S., and Yang, Q. S. (2012). "Experimental research on mechanical properties of timber in ancient Tibetan building," *Journal of Materials in Civil Engineering* 24(6), 635-643. DOI: 10.1061/(ASCE)MT.1943-5533.0000438

Yin, W. D., and Yamamoto, H. (2013). "Standing tree assessment for the maintenance of historic wooden buildings: A case study of a World Heritage Site in China," *Journal of Biogeosciences and Forestry* 6(4), 169-174. DOI: 10.3832/ifor0753-006

Zhang, J., Wang, Y. C., Xu, Q. F., Yang, X. J., and Li, X. M. (2011). "Residual strength of service-beyond wood members of Douglas fir and cedarwood using non-destructive testing," *Journal of Central South University (Science and Technology)* 42(12), 3864-3870.

Article submitted: February 16, 2015; Peer review completed: April 19, 2015; Revised version received and accepted: May 17, 2015; Published: May 21, 2015.
DOI: 10.15376/biores.10.3.4167-4177